Impedimetric biosensor for detection of cancer cells employing carbohydrate targeting ability of Concanavalin A

Ankan Dutta Chowdhury, Akhilesh Babu Ganganboina, Enoch Y. Park, Ruey-an Doong

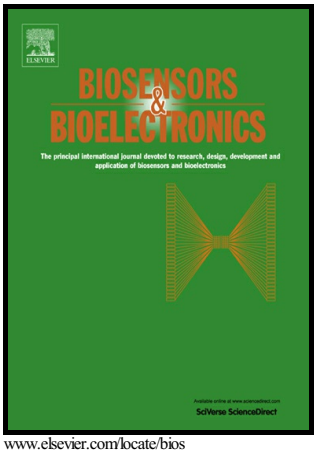

www.elsevier.com/locate/bios

PII: S0956-5663(18)30635-3
DOI: https://doi.org/10.1016/j.bios.2018.08.039
Reference: BIOS10703

To appear in: *Biosensors and Bioelectronic*

Received date: 22 May 2018
Revised date: 30 July 2018
Accepted date: 16 August 2018

Cite this article as: Ankan Dutta Chowdhury, Akhilesh Babu Ganganboina, Enoch Y. Park and Ruey-an Doong, Impedimetric biosensor for detection of cancer cells employing carbohydrate targeting ability of Concanavalin A, *Biosensors and Bioelectronic,* https://doi.org/10.1016/j.bios.2018.08.039

Impedimetric biosensor for detection of cancer cells employing carbohydrate targeting ability of Concanavalin A

Ankan Dutta Chowdhury[a 1], Akhilesh Babu Ganganboina[b], Enoch Y. Park[c,d], Ruey-an Doong[a,b,*]

[a]Institute of Environmental Engineering, National Chiao Tung University, 1001 University Road, Hsinchu, 30010, Taiwan

[b]Department of Biomedical Engineering and Environmental Sciences, National Tsing Hua University, 101 Section 2, Kuang-Fu Road, Hsinchu, 30013, Taiwan

[c]Laboratory of Biotechnology, Research Institute of Green Science and Technology, Shizuoka University, 836 Ohya, Suruga-ku, Shizuoka 422-8529, Japan

[d]College of Agriculture, Academic Institute, Shizuoka University, 836 Ohya, Suruga-ku, Shizuoka 422-8529, Japan

[*]Corresponding author: radoong@mx.nthu.edu.tw

[1] ADC: present address is Laboratory of Biotechnology, Research Institute of Green Science and Technology, Shizuoka University, 836 Ohya, Suruga-ku, Shizuoka 422-8529, Japan.

Abstract

The successful development of selective detection of cancer cells from normal cells is a highly demanded but challenging task. Herein, we have developed a rapid and label-free impedimetric biosensor for quantitative determination of cancer cells with high glycoprotein expression. Homogenously distributed 2 – 9 nm graphene quantum dots (GQDs) was anchored on the surface Fe_3O_4 through covalent bonding. Concovalin A (ConA) was then adhered onto GQDs by physical mixing to fabricate ConA-GQD@Fe_3O_4 nanosensing probe. A good dynamic range in the cell concentration of $5 \times 10^2 - 1 \times 10^5$ cells mL^{-1} with LOD values of 246 and 367 cells mL^{-1} for HeLa and MCF-7, respectively, is obtained. The impedimetric responses to the cancerous HeLa and MCF-7 cells are 16.7 and 13.1 times higher than those of their original sensor electrodes. However, the interaction between sensing probe and normal MCF-10 and bEnd.3 cells is negligible, confirming the specific selectivity toward cancer cells. Cellular uptake images as well as in-vitro cytotoxicity corroborates the electrochemical results. In addition, the successful detection of cancer cells in human serum and circulating tumor cells in blood sample envisions the feasibility of using ConA-GQD@Fe_3O_4 as the nanosensing probe for clinically early diagnosis of cancer cells with high glycoprotein expression.

Keywords: Impedimetric biosensor; cancer cell detection; concanavalin A (ConA); label-free; graphene quantum dots (GQDs).

1. Introduction

The development of promising biosensing materials for rapid and accurate diagnosis of diseases from simple fever to malignant tumor has become one of the important issues for biomedical application (Chen et al., 2013; Chowdhury et al., 2014; Dutta Chowdhury et al., 2017; Hsu et al., 2016). When shaping the research trends in the past decades, it can be found that the development of novel biosensor has provided a rapid and reliable tool to identify and quantify the target analytes in the presence of a wide variety of matrices (Ganganboina et al., 2017b; Qureshi et al., 2012; Shao et al., 2010; Tsai and Doong, 2005). In particular, the use of cancer markers for the development of detection techniques has been widely employed, which can produce rapid and multiplexed detection of several diseases with high sensitivity (Chowdhury et al., 2018; Ho et al., 2015; Lee et al., 2007). Numerous serum tumor markers including MUC-1 family of mucin glycoproteins, α-fetoprotein and prostate-specific antigen have been well established for the quantitative detection of breast, liver, and prostate cancers, respectively (Cui et al., 2016; Jia et al., 2016; Pan et al., 2017; Parshetti et al., 2013). However, their application in cancer detection is controversial largely due to the lack of specificity to meet diagnostic criteria. Therefore, the development of simple and rapid biosensing technology with specificity for direct cancerous cells is urgently needed.

Nanomaterials have been demonstrated to be promising materials to enhance the detection selectivity and sensitivity of biosensors. Graphene quantum dots (GQDs) (Anh et al., 2017; Dutta Chowdhury and Doong, 2016; Shao et al., 2010; Zhou et al., 2015) and gold nanoparticles (AuNPs) (Chiu et al., 2015; Huang et al., 2017) have been reported to effectively deliver optical as well as electrochemical signals for *in vivo* or in vitro biosensing purposes. Moreover, the functionalization of GQDs and AuNPs with biomolecules such as antibody,

antigen and aptamer can improve their ability towards specific tumor cell detection. Liu et al. (2009) have used aptamer-coated AuNPs to effectively detect cancer cells. GQDs entrapped with folic acid have also been investigated to detect and image cancer cells by exploiting the specific interaction of folic acid receptor with GQDs (Wang et al., 2014b). Hong et al. (2015) have recently prepared a highly sensitive electrochemical sensor for cancer cell detection using Concanavalin A (ConA) as the sensing probe. ConA is one of the carbohydrate-binding proteins originally extracted from *Canavalia ensiformis* (jack bean), which are highly specific to bind sugar moiety of carbohydrates including sugar, glycoprotein and glycolipid. Since diseases associated with glycosylation alteration in glycoproteins and glycolipids play a crucial role in most cancer cell formation (Zhao et al., 2007), the high and specific affinity of ConA toward sugar moiety can thus serve as the sensitive and selective sensing probe for rapid detection of cancer cells with high glycoprotein expression.

In this work, we have developed a label-free electrochemical biosensor for rapid detection of cancer cells using ConA-GQD@Fe_3O_4 as the biosensing electrode material. The approach of targeting cancer cells has been achieved by using ConA to probe the glycoprotein or glycopeptide on the surface of cancer cells, which can produce accurate signal on the *in-vitro* cancerous environment. As shown in Scheme 1, ConA-GQD is covalently bonded with APTES-functionalized Fe_3O_4 nanoparticles through EDC/NHS chemistry and the ConA-GQD@Fe_3O_4 nanocomposites coated onto Au electrode has been used for electrochemical impedance spectroscopic (EIS) analysis. The sensing electrode is incubated with different types of cells including cancerous HeLa and MCF-7 cells and non-cancerous MCF-10 and endothelial (bEnd.3) cells. The normal cell lines of MCF-10 and bEnd.3 are selected as the control for specific cancer cell detection because of their low membrane-associated

glycoprotein structure. An excellent linear relationship between impedance and cancerous cell concentration with the limit of detection of 246 cells mL^{-1} for HeLa and 367 cells mL^{-1} for MCF-7 is observed, which exhibits the simplicity and sensitivity of the label-free ConA-based biosensors for accurate detection of cancerous cells. Cellular uptake images as well as *in-vitro* cytotoxicity are also carried out to check the bio-applicability of the nanocomposites. In addition, the successful detection of the cancerous cells in human serum and circulating tumor cells (CTC) in blood samples by Au||ConA-GQD@Fe_3O_4 electrode envisions that the developed approach could be applied clinically for ultra-early diagnosis and monitoring of cancer cells with high glycoprotein expression.

2. Materials and methods

2.1 Materials

$FeCl_3 \cdot 6H_2O$, $FeSO_4 \cdot 7H_2O$, citric acid, (3-aminopropyl)triethoxysilane (APTES), sodium dihydrogen phosphate, disodium hydrogen phosphate and *N*-(3-(dimethylamino)propyl)-*N*′-ethylcarbodiimide hydrochloride (EDC) were purchased from Sigma-Aldrich (St. Louis, MO). *N*-hydroxysuccinimide (NHS) was obtained from Alfa Aesar (Lancashire, UK). $K_3Fe(CN)_6$ and $K_4Fe(CN)_6$ were from J. T. Baker (Phillipsburg, NJ). ConA from *Canavalia ensiformis* was purchased from Sigma (St. Louis, US). Gold disk electrodes and alumina powders (0.2 and 0.05 mm) were purchased from Metrohm AG (Ionenstrasse, Switzerland). Analytical grade of toluene and other reagents were used as received without further purification. All the solutions were prepared by using Milli-Q water (18.2 MΩ cm) unless otherwise mentioned.

2.2 Synthesis of GQDs

GQDs were synthesized using our previously reported method (Dutta Chowdhury and Doong, 2016). In brief, 2 g of citric acid were heated into a 200-mL round bottom flask to 200°C for 30 min until the color of solution changed to orange liquid. The solution was then transferred into 100 mL of 10 mg mL^{-1} NaOH solution drop-wisely and then purified by dialysis bag of 1 kDa for 24 h to remove un-reacted citric acid.

2.3 Synthesis of GQD@Fe_3O_4

The magnetic Fe_3O_4 nanoparticles were prepared by standard co-precipitation method using $FeCl_3 \cdot 6H_2O$ and $FeSO_4 \cdot 7H_2O$ salts at the ratio of 2:1 in the presence of N_2 gas (Wang et al., 2014a). To functionalize the as-synthesized Fe_3O_4, APTES was hydrolyzed first and then coated onto the surface of magnetic Fe_3O_4 nanoparticles (Ganganboina et al., 2017a). The precipitate was washed several times with fresh toluene and then magnetically separated and dried at 60°C under vacuum. The GQD@Fe_3O_4 was synthesized by adding 10 mL of 50 µg mL^{-1} as-synthesized GQDs to 10 mg of APTES coated Fe_3O_4 nanoparticles in the presence of 3 mg of EDC and 5 mg of NHS (Valeur and Bradley, 2009).

2.4 Characterization

The high resolution transmission electron microscopy (HRTEM) was used to identify the morphology and size of GQDs and Fe_3O_4-based nanomaterials by using a JEOL JEM-2010 high-resolution TEM at 200 kV (Tokyo, Japan). X-ray photoelectron spectroscopy (XPS) was performed with an ESCA Ulvac-PHI 1600 photoelectron spectrometer from Physical Electronics using Al Kα radiation photon energy at 1486.6 ± 0.2 eV (Physical Electronics,

Eden Prairie, MN). The thermal property of nanomaterials was examined by thermogravimetric analysis (TGA) using Mettler Toledo DSC/TGA 3+ Stare system in the presence of N_2. The hydrodynamic diameter of GQDs, Fe_3O_4 and GQD@Fe_3O_4 nanoparticles in aqueous solutions was determined by a Zetasizer Nano ZS dynamic light scattering (DLS) (Malvern Inst. Ltd., UK). Electrochemical characterization of cyclic voltammetry (CV) and electrochemical impedance spectroscopy (EIS) were carried out on an Autolab PGSTAT 302N potentiostat/galvanostat electrochemical test system (Metrohm B.V., Switzerland) in a conventional three-electrode cell consisting with an Au disk electrode (2 mm in diameter), platinum wire and saturated Ag/AgCl as the working, auxiliary, and reference electrodes, respectively.

2.5 Preparation of ConA-GQD@Fe_3O_4 electrode

The ConA-GQD@Fe_3O_4 based electrode was prepared by dissolving ConA in PBS buffer at pH 7.0 with required concentration and store at 4°C for 4 h for activation. The GQD@Fe_3O_4 was then incubated with 1 mL of activated ConA at room temperature for 2 h. To prepare the sensing electrode, 5 mg of ConA-GQD@Fe_3O_4 nanocomposites were mixed with few drops of PVDF binder and 10% of carbon black powder. 10 µL of the mixture were then added onto the washed Au milli-electrode surface at room temperature for 1 h. After that, the electrode surface was washed thoroughly with Milli-Q water and then dried under nitrogen stream. Moreover, the pure Au, Au|| Fe_3O_4 and Au|| GQD@Fe_3O_4 electrodes were also prepared to serve as the blank electrodes to elucidate the role of GQDs in cancer cell detection.

2.6 Cell culture and sample preparation

The cancerous and normal cells were cultivated using the standard protocols. Briefly, HeLa, MCF-7 and bEnd.3 cells were maintained in DMEM media (Gibco, Rockville, MD, USA) supplemented with 100 kU mL^{-1} of penicillin at 37 °C in a humidified 5% CO_2-in-air atmosphere. MCF-10 cells were cultured under the same conditions except the use of MEBM medium containing 1% of 100 kU mL^{-1} penicillin. All types of cells were collected by centrifuge at 2000 rpm for 10 min from the culture medium and washed by 100 mM phosphate buffer saline solution (PBS) at pH 7.4. The cell numbers were calculated and then adjusted to 100,000 cells mL^{-1} as the stock solution. Then, the cells were serial diluted in PBS buffer to 6 various cell concentrations of 100000, 50,000, 10,000, 5,000, 1,000, and 500 cells mL^{-1} for biosensing measurements.

2.7 Electrochemical characterizations and sensing of cells

Glucose, the surrogate of carbohydrate moiety, was primarily used in this study to characterize the cyclic voltammetric (CV) performance of as prepared Au||ConA-GQD@Fe_3O_4 electrode in 10 mM PBS solution at pH 7.4 containing 100 mM NaCl and 5 mM $K_3Fe(CN)_6^{3-/4-}$. Electrochemical impedance spectroscopy (EIS) of the Au||ConA-GQD@Fe_3O_4 electrode was carried out with an applied potential of 5 mV across the electrodes over the frequency range of 100 kHz – 0.1 Hz with an Autolab impedance analyzer. Both the cancerous and normal cell sensing processes were carried out by immersing the sensor electrode into the PBS solution containing 6 various concentrations of cells for 10 min in order to attach the cells to the ConA surface.

2.8 Cell images of ConA-GQD@Fe_3O_4

To understand the effect of cellular uptake by ConA-GQD@Fe_3O_4 nanocomposites in fluorescence microscopy imaging (Olympus, IX70, Tokyo, Japan), cells were initially seeded on a 2 cm × 2 cm glass cover slips in a six well plate at the concentration of 1×10^6 cells per well at 37 °C. Then, the cells were treated with 20 μg mL^{-1} ConA-GQD@Fe_3O_4 for 4 h, and then washed with PBS solution twice. Finally, the cells were then fixed with mounting gel and the cover slips were covered with micro-slides to take the images.

3. Results and discussion

3.1 Characterisation of GQDs and ConA-GQD@Fe_3O_4 nanocomposites

In this study, GQDs were synthesized from citric acid via pyrolysis according to our previous study (Dutta Chowdhury and Doong, 2016). The TEM image of GQDs shown in Fig. 1A confirms the homogenous distribution of GQDs where the sizes are 2 – 9 nm in diameter with a mean particle size of 6.0 ± 0.5 nm (Fig. 1B). The measured lattice spacing of 0.21 nm is found in the high resolution TEM image (Fig. 1C), which corresponds to the (100) lattice plane of the defect free graphene layer (Jia and Ji, 2015). The colour of transparent GQDs solution changes from colourless to blue, indicating its excellent fluorescence property (Fig. S1, Supplementary data).

Magnetite Fe_3O_4 nanoparticles is chosen as the core support in this study because of its simple synthesis, low cost, and good matrix for GQD anchoring. The TEM image shows that the average diameter of Fe_3O_4 nanoparticles is 23 nm (Fig. 1D). To functionalize the Fe_3O_4 nanoparticle surface, silanization with APTES was carried out to introduce $–NH_2$ group onto the Fe_3O_4 surface. In addition, the silane coating can decrease the magnetic susceptibility as

well as the aggregation of particles, which is beneficial for sensor preparation as it can load more GQDs onto the surface of Fe_3O_4. The TEM image of GQD@Fe_3O_4 nanocomposite shows the conjugation of Fe_3O_4 nanoparticles with GQDs (Fig. 1E). Moreover, the agglomeration of Fe_3O_4 nanoparticles is reduced significantly after the formation of nanocomposite due to the coating of APTES and GQDs onto the surface. In addition, two different fringes are clearly observed in the GQD@Fe_3O_4 nanocomposite (Fig. 1F), indicating the successful co-existence of GQDs along with Fe_3O_4 nanoparticles. The corresponding fringes of GQDs (0.21 nm) (Dutta Chowdhury and Doong, 2016) and Fe_3O_4 (0.26 nm) (Wu et al., 2012) are deciphered, confirming the successful formation of GQD@Fe_3O_4.

XPS was used to identify the change in elemental environment before and after the loading of GQDs onto Fe_3O_4 nanoparticles. As shown in Fig. 1G, the survey spectrum of Fe_3O_4 shows the standard peaks of O 1s (532 eV) and Fe 2p (710 and 724 eV) (Lin and Doong, 2011). A small hump of carbon peak (C 1s) at 284 eV appears due to the adventitious carbon sources. After surface modification with GQDs, the peak intensity of C 1s increases and an additional peak of N 1s at 400 eV is clearly observed in the survey scan of GQD@Fe_3O_4 nanocomposite, indicating the presence of amine group of APTES (Li et al., 2015). To explore the nitrogen linkage in the GQD@Fe_3O_4 nanocomposites, the N 1s peak is further deconvoluted. As shown in Fig. 1H, a significant contribution of C–N at 401.7 eV over N–H peak (399.4 eV) is observed. The predominant C–N peak is contributed from the successful formation of amide group between –COOH of GQDs, while N–H peak is mainly from the $–NH_2$ of APTES linked with Fe_3O_4. Similarly, the deconvoluted peak of Fe 2p of GQD@Fe_3O_4 nanocomposite shows Fe^{2+} and Fe^{3+} peaks at 710.6 and 712.8 eV, respectively, which is located at the same position in comparison with the bare Fe_3O_4 (Fig. S2,

Supplementary data). This result proves that the GQDs are only loaded onto the functionalized surface and have little influence on the core structure of Fe_3O_4,

The thermal property of GQD@Fe_3O_4 along with the as-prepared Fe_3O_4 was carried out in N_2 to estimate the loading amount of GQDs (Fig. 1I). The total weight loss of as-prepared Fe_3O_4 and GQD@Fe_3O_4 is found to be 3.6 and 11.2 wt%, respectively. The significant weight loss of as-prepared Fe_3O_4 at 260–370°C is associated with the dehydroxylation of structural Fe-O, which is highly corroborated with the reported data (Xie et al., 2007). An additional 7.6 wt% loss of GQD@Fe_3O_4 nanocomposites at 350 – 430 °C in comparison with the bare Fe_3O_4 can be assigned as the attached amount of GQDs and APTES in nanocomposites (Ganganboina et al., 2017a), which supports the attachment of GQDs and APTES layer on Fe_3O_4 nanoparticles. Besides, the mean hydrodynamic diameter of GQDs and as-prepared Fe_3O_4 is 57 and 436 nm with PDI of 0.16 and 0.21, respectively (Fig. 1J). The large diameter of as-prepared Fe_3O_4 is mainly attributed to the agglomeration of magnetic Fe_3O_4 (Patra et al., 2015). However, the successful coating of APTES followed by the GQD attachment increases the dispersive nature of nanocomposites in aqueous phase, and then decreases the mean hydrodynamic diameter of ConA-GQD@Fe_3O_4 to 198 nm, which makes the system more facile for sensor application as well as for cell interaction.

3.2 Fabrication and characterizations of sensor electrode

To optimize the loading of ConA on the GQD@Fe_3O_4 coated Au electrode, CV was performed in $K_3Fe(CN)_6^{3-/4-}$ system in a potential window ranging of -0.2 – 0.6 V at a scan rate of 0.01 V s^{-1}. As shown in Fig. 2A, the peak intensity of $Fe(CN)_6^{3-/4-}$ in PBS buffer decreases when the loading of ConA onto GQD@Fe_3O_4 increases from 50 nM to 1 µM. The

decreasing tendency in peak intensity obtained from CV curve is conclusive to the electroactivity of the developed sensing probe. The peak intensity of $Fe(CN)_6^{3-/4-}$ at +0.16/+0.27 V of the Au||GQD@Fe_3O_4 electrode decreases gradually along with the increasing concentration of ConA. This phenomenon is mainly attributed to the fact that the charge transfer between electrolyte and the surface of Au||GQD@Fe_3O_4 electrode is hindered partially by the immobilization of big sized ConA molecule. Since the high loading amount of ConA can make sensor probe more specific toward cancer cell surface, the increase in ConA loading is attempted. At the concentration of 1 µM ConA, the CV response reduces intensely which is not suitable for the electrochemical application due to the poor electroactivity. However, the loading of 500 nM ConA onto GQD@Fe_3O_4 surface exhibits the sufficient electroactivity with moderately well loaded ConA amount. Therefore, 500 nM of Con A is selected as the optimized immobilization concentration on the GQD@Fe_3O_4 nanocomposite for the further study on cancer cell detection. It is noteworthy that GQDs, being a zero dimensional and electroactive nanomaterial, have been reported as a potential matrix for electrochemical applications (Ganganboina et al., 2017a; 2017b). The homogeneous distributed GQDs in GQD@Fe_3O_4 nanocomposites are well-accepted as the successful cargo for ConA molecules to form GQD-ConA conjugate because of its electron enriched surface. Moreover, the Fe_3O_4 nanoparticle is chosen as the core support of GQD anchoring, which can be coated onto the electrode surface easily to make the sensor electrode rigid. Moreover, the magnetic behaviour of ConA-GQD@Fe_3O_4 can be served as a suitable carrier for *in vitro* analysis of cancer cells in the future in the presence of external magnetic moment force.

3.3 Glucose binding assay

The electrochemical performance of ConA loaded GQD@Fe_3O_4 sensor (Au||ConA-GQD@Fe_3O_4) was first examined by CV in the presence of various concentrations of glucose and $K_3Fe(CN)_6^{3-/4-}$ prior to the cancer cell detection. As shown in Fig. 2B, the redox peak intensity of $Fe(CN)_6^{3-/4-}$ is highly sensitive toward glucose concentration. The peak intensity decreases gradually with the increase in glucose concentration ranging from 10 to 500 nM. This is mainly attributed to the fact that the successful attachment of glucose on the Au||ConA-GQD@Fe_3O_4 electrode surface would generate the non-conducting layer of attached glucose, resulting in the restriction of electron transfer processes on the electrode surface. This clearly indicates the excellent binding ability of immobilized ConA toward the sugar moiety.

3.4. Specific detection of cancer cells by EIS

In order to develop the label free cancer cell detection technique, a three-electrode electrochemical chamber in PBS buffer at pH 7.4 was used to investigate the impedimetric behaviors of Au||ConA-GQD@Fe_3O_4 electrode before and after the attachment of different cell lines. Four types of cells including cancerous HeLa and MCF-7 cells and normal MCF-10 and bEnd.3 cells were used to evaluate the specificity of the developed impedimetric sensors. The Nyquist plots of Au||ConA-GQD@Fe_3O_4 electrode in the presence of 4 different cell lines with various concentrations are given in Fig. 2C-F. It is clear that the diameter of semicircle, which represents the charge transfer resistance (R_{ct}), becomes large after the attachment of cells, which indicates the increase in resistance caused by the large-sized cell onto the electrode surface. Moreover, the diameter of semicircle increases with the increase in cell concentration from 5×10^2 to 1×10^5 cells mL^{-1}. It is also interesting to note that the

Au||ConA-GQD@Fe_3O_4 electrode shows the significant enhancement on impedance after incubation with cancerous HeLa (Fig. 2C) and MCF-7 cells (Fig. 2D), while no obvious resistance increment is observed for noncancerous bEnd.3 (Fig. 2E) and MCF-10 cells (Fig. 2F) under the identical conditions.

To validate the role of ConA, the electrode without the loading of ConA (Au||GQD@Fe_3O_4 electrode) is also tested with the both cell lines at 10^5 cells mL^{-1} (Fig. S3, Supplementary data). Few cells are attached on the Au||GQD@Fe_3O_4 electrode surface by weak electrostatic interaction due to the π-delocalization of the GQDs surface. After the addition of HeLa and bEnd.3 cells, the R_{ct} of the Au||GQD@Fe_3O_4 electrode increases to 4.76 and 4.56 kΩ, respectively, that is 9 times higher than that of the bare Au||GQD@Fe_3O_4 electrode in the absence of cell. This increment is much lower in comparison with the Au||ConA-GQD@Fe_3O_4 electrode, which is 32 times higher than the bare electrode at 10^5 cells mL^{-1} HeLA cells. It is noteworthy that the R_{ct} value between HeLa and bEnd.3 cells are similar (4.76 and 4.56 kΩ), depicting that the selectivity of Au||GQD@Fe_3O_4 electrode toward cancer cell detection is low. Moreover, the bare Au and Au||Fe_3O_4 electrodes were also used as the control electrodes. As shown in Fig. S4 (Supplementary data), the attachment of HeLa cells onto both bare Au and Au||Fe_3O_4 electrodes is insignificant, which is similar to those of bare electrodes without the addition of cell. Moreover, little difference in R_{ct} between cancer HeLa and noncancerous bEnd.3 cells is observed. These results clearly indicate that ConA not only activates the specificity toward cancer cell detection but also increases the cell attachment.

After examining several possible equivalent circuit scenarios, a best-fitted diagram over the frequency range of 10 kHz – 0.1 Hz is illustrated in the inset of Fig. 2C. The fitted

parameters for Nyquist plots of HeLa cells are shown in Table S1 (Supplementary data). A significant change in R_{ct} is observed after the entrapment of cell concentrations. The initial value of the charge transfer resistance is 0.51 kΩ, which can be primarily contributed from the electron transfer between ConA-GQD@Fe_3O_4 and PBS electrolyte. After the entrapment of various concentrations of HeLa cells, the surface of ConA–GQD is covered with cells and results in the increase in charge transfer resistance up to 15.31 kΩ at 10^5 HeLa cells mL^{-1}. Similar trends is also reported for bacterial and cell detection systems (Chowdhury et al., 2012; Hong et al., 2015; Hu et al., 2013). The solution resistance for all the concentrations of HeLa cell shows a constant value (Table S1), presumably attributed to that the charge transfer as well as ion movement process could not alter the mobile ion concentration in the electrolyte solution.

To further evaluate the sensor specificity, total impedance, $Z_{tot} = (Z_{real}^2 + Z_{ima}^2)^{0.5}$ in the selected frequency range of 1 – 10 kHz of all four types of cells are presented in Fig. 3 (A-D). A well-defined result is found for cancerous HeLa and MCF-7 cells in the concentration range of $5 \times 10^2 – 1 \times 10^5$ cells mL^{-1} (Figs. 3A and 3B). Fig. 3E shows the comparative bar diagram of change in total impedance as a function of four types of cell line concentration. For cancerous HeLa and MCF-7 cells, a 16.7 and 13.1 fold increase in total impedance with respect to their corresponding bare Au||ConA-GQD@Fe_3O_4 electrodes is observed. Moreover, the limit of detection (LOD), determined by 3 × standard deviation of lowest concentration divided by slope of the calibration line, of 246 and 367 cells mL^{-1} for Hela and MCF-7, respectively, is obtained. In contrast, the normal cells of MCF-10 and bEnd.3 only show 1.7 and 2.8 fold increase, respectively, in the concentration range of $0 – 10^5$ cells mL^{-1}. The big difference in impedance between cancerous and normal cells clearly indicates the high specific

nature of the Au||ConA-GQD@Fe_3O_4 sensor electrode toward cancer cell detection. In addition, the specificity of the developed biosensing probe on cancer cell detection with low LOD and wide linear range makes the ConA-GQD@Fe_3O_4 a superior impedimetric sensing material for cancer cell detection with high glycoprotein expression.

The effectiveness of the Au||ConA-GQD@Fe_3O_4 electrode on the detection of cancer cells in complex matrix is also validated using 10^3 – 10^5 cell mL^{-1} of HeLa cell in human serum. As shown in Fig. S5 (Supplementary data), the R_{ct} of bare Au||ConA-GQD@Fe_3O_4 electrode is found to be 1.45 kΩ in serum samples, which is little higher than that in PBS buffer (Fig. 2C). In addition, the R_{ct} value of HeLa cells in human serum is 4.3 kΩ at 10^3 cell mL^{-1}, 12.8 kΩ at 10^4 cell mL^{-1} and 16.6 kΩ at 10^5 cells mL^{-1}, which is higher than those in PBS buffer at the same concentration of HeLa cells. These results clearly indicate the matrix effect of human serum. However, the good relationship between the change in total impedance and HeLa cell in human serum is still observed, which validate the applicability of the Au||ConA-GQD@Fe_3O_4 electrode to cancer cell detection in human serum.

Table 1 compares the analytical performance of Au||ConA-GQD@Fe_3O_4 with the recently reported cancer cell detection sensors. Several studies have utilized immobilized antibody or aptamer based biosensor for specific detection of cancer cells or markers to enhance the detection sensitivity. Although the detection sensitivity can be lower to 8 – 30 cells mL^{-1} using DPV method, these biosensors need expensive antibody or aptamers, which are sensitive to storage conditions (Tabrizi et al., 2017; Wang et al., 2017; Zhang et al., 2018). In contrast, the developed Au||ConA-GQD@Fe_3O_4 biosensors in this study can achieve high selectivity for cancer cell detection based on the principle of high affinity binding of cancerous cells to ConA without the utilization of expensive biomolecules. Moreover, the reported LOD

values of antibody/aptamer based biosensors are in the range of 100 – 6000 cells mL^{-1} when EIS method are used (Chen et al., 2016; Feng et al., 2011; Pan et al., 2009; Seven et al., 2013), which is comparable with our results. These results clearly indicate the excellence of ConA-GQD@Fe_3O_4 as a promising nanosensing probe for sensitive and selective detection of cancer cells with high glycoprotein expression. It is noteworthy that the developed biosensor has a limitation for general cancer cell detection because sometimes glycoprotein expression of cancer cell is relatively lower than normal cells. However, most cancer cell can overexpress glycoproteins or glycoaldose in comparison with normal cells, making the developed impedimetric biosensor available for the detection of cancer cells.

3.5 Cellular uptake of ConA-GQD@Fe_3O_4 nanocomposite

To establish the specific cell attachment of ConA-GQD@Fe_3O_4, cell imaging assay was performed in two different cell lines, i.e., cancerous HeLa cells and non-cancerous bEnd.3 cells. As shown in Fig. 3F, the fluorescence of GQDs in HeLa cells (Fig. 3Fi) is are considerably stronger than that in the normal bEnd.3 cells (Fig. 3Fii). This result reflects the specific attachment of ConA-GQD to HeLa cells, which is consistent with the fact that HeLa cells can overexpress glycoprotein and glycolipids, while normal bEnd.3 express at a low level. A previous study has depicted that GQD can load with drug molecules via its nano-dimensional surface and then deliver into cancer cells through the pH-mediated process (Qiu et al., 2015). This indicates that the ConA-GQD can be used as a selective cell imaging agent as well as a drug delivery carrier in the future. The ConA-GQD@Fe_3O_4 can be applied to conjugate drugs with a wide variety of biomolecules, and visualize their effect without interfering with their biological functions. Moreover, the *in-vitro* cytotoxicity of as-

synthesized GQDs and ConA-GQD@Fe_3O_4 nanocomposites were evaluated with Hela cells by MTT assay. As shown in Fig. S6 (Supplementary data), both GQDs and GQDs-ConA@Fe_3O_4 show low toxicity toward HeLa cells, and the cell viability is higher than 80 % when 20 µg mL^{-1} of nanomaterials are used. The images also show that ConA-GQD@Fe_3O_4 can clearly label the cytoplasm because of the fluorescence property of GQDs whereas the incorporation of ConA to the nanocomposite can accumulate more sensing materials on cancerous HeLa cells in comparison with normal cells to enhance the sensitivity and selectivity of electrode.

3.6. Detection of circulating cancer cells (CTC)

As the CTC can serve a promising analyte to track cancer evolution, the detection of CTC by the Au||ConA-GQD@Fe_3O_4 electrode is one of the most reliable and attractive strategies to understand the applicability of the proposed sensor for clinic diagnosis. In this study, 1000 cell mL^{-1} CTC in PBS buffer was used to verify the effectiveness of the Au||ConA-GQD@Fe_3O_4 biosensing electrode. Fig. 4A shows the Nyquist plot of Au||ConA-GQD@Fe_3O_4 electrode after the addition of CTC with its dilution. The CTC-loaded electrode shows the R_{ct} value of 4.4 kΩ in 10-time diluted solution and then increases to 11.4 kΩ for as received CTC. The total impedance plot illustrated in Fig. 4B also reflects the same pattern. Since the cell concentration of CTC is highly dependent on the metastasis stage of cancer development and is hard to get the sufficient amount for calibration, the calibration curve of HeLa cell in PBS buffer was used to estimate the CTC concentration. It is clear that the CTC concentration by Au||ConA-GQD@Fe_3O_4 electrode is calculated to be 1215 cell mL^{-1}, which is similar to the added amounts of original CTC concentration (1000 cell mL^{-1}). Moreover, the

CTC concentration after 10 × dilution is 307 cell mL^{-1}. This value is close to the detection limit of the biosensing probe, clearly indicating the feasibility of the developed biosensing probe for the effective and reliable detection of cancer cells.

4. Conclusions

In this study, we have successfully developed a label-free biosensor for sensitive detection of cancer cells. The synthesized ConA-GQD@Fe_3O_4 nanocomposites serve as the impedimetric biosensing platform to sensitively and selectively detect cancerous HeLa and MCF-7 cells. A 16.7 and 13.1 fold increase in impedance for cancerous HeLa and MCF-7 cells is observed, which is 4.7 – 9.8 times higher than those of normal cells of MCF-10 and bEnd.3. In addition, a dynamic linear range of $5 \times 10^2 – 1 \times 10^5$ cells mL^{-1} with LOD values of 246 and 367 cells mL^{-1} for HeLa and MCF-7, respectively, is achieved, confirming the specific detection ability of the sensor. The detection principle of the developed biosensing probe exhibits the specific binding ability of ConA toward the glycogenated cancer cell surface with glycoproteins and aldose overexpression, making ConA-GQD@Fe_3O_4 nanocomposite a major advantage over other reported aptamers and antibody based sensing techniques. Moreover, the cellular uptake images of ConA-GQD@Fe_3O_4 nanocomposite confirm the attachment of ConA-GQD@Fe_3O_4 to cancerous HeLa cells with more intensity compared with normal bEnd.3 cells under the identical condition. Results obtained from CTC measurement has extended the role of electrochemically impedimetric method in determining the cancer cells using ConA-GQD@Fe_3O_4 nanocomposite as the biosensing probe, which can extend the platform for its biomedical applications such as drug delivery and bioimaging in the future.

Acknowledgement

The authors thank the Ministry of Science and Technology (MOST), Taiwan for financial support under grant Nos. 104-2221-E-009-020-MY3 and 105-2113-M-009-023-MY3. ADC is acknowledged to the Ministry of Science and Technology (MOST), Taiwan and then Japan Society for the Promotion of Science (JSPS), Japan for financial support.

References

Anh, N.T.N., Chowdhury, A.D., Doong, R.A., 2017. Sens. Actuators, B 252, 1169-1178.

Chen, L.-Y., Huang, C.-C., Chen, W.-Y., Lin, H.-J., Chang, H.-T., 2013. Biosens. Bioelectron. 43, 38-44.

Chen, X., Pan, Y., Liu, H., Bai, X., Wang, N., Zhang, B., 2016. Biosens. Bioelectron. 79, 353-358.

Chiu, W.-J., Ling, T.-K., Chiang, H.-P., Lin, H.-J., Huang, C.-C., 2015. ACS Appl. Mater. Inter. 7, 8622-8630.

Chowdhury, A.D., Agnihotri, N., De, A., Sarkar, M., 2014. Sens. Actuators, B 202, 917-923.

Chowdhury, A.D., De, A., Chaudhuri, C.R., Bandyopadhyay, K., Sen, P., 2012. Sensors and Actuators B: Chemical 171, 916-923.

Chowdhury, A.D, Ganganboina, A. B., Tsai, Y. C., Chiu, H.C., Doong, R.A., 2018. Anal Chem Acta. 1027, 109-120.

Cui, Z., Chen, Y., Xiao, Z., Hu, M., Lin, Y., Chen, Y., Zheng, Y., 2016. Oncotarget 7, 25791.

Dutta Chowdhury, A., Agnihotri, N., Doong, R.A., De, A., 2017. Anal. Chem. 89, 12244-12251.

Dutta Chowdhury, A., Doong, R.A., 2016. ACS Appl. Mater. Inter. 8, 21002-21010.

Feng, L., Chen, Y., Ren, J., Qu, X., 2011. Biomaterials 32, 2930-2937.

Feng, Q.-M., Liu, Z., Chen, H.-Y., Xu, J.-J., 2014. Electrochem. Commun. 49, 88-92.

Ganganboina, A.B., Chowdhury, A.D., Doong, R.A., 2017a. Electrochim. Acta. 245, 912–923.

Ganganboina, A.B., Dutta Chowdhury, A., Doong, R.A., 2017b. ACS Appl. Mater. Inter. 10, 614–624.

Guo, Y., Shu, Y., Li, A., Li, B., Pi, J., Cai, J., Cai, H.H., Gao, Q., 2017. J. Mater. Chem. B 5, 5532-5538.

Ho, L.-C., Wu, W.-C., Chang, C.-Y., Hsieh, H.-H., Lee, C.-H., Chang, H.-T., 2015. Anal. Chem. 87, 4925-4932.

Hong, S.A., Kwon, J., Kim, D., Yang, S., 2015. Biosens. Bioelectron. 64, 338-344.

Hsu, C.-L., Lien, C.-W., Wang, C.-W., Harroun, S.G., Huang, C.-C., Chang, H.-T., 2016. Biosens. Bioelectron. 75, 181-187.

Hu, Y., Zuo, P., Ye, B.-C., 2013. Biosens. Bioelectron. 43, 79-83.

Huang, J.-Y., Lin, H.-T., Chen, T.-H., Chen, C.-A., Chang, H.-T., Chen, C.-F., 2017. ACS Sensors 3, 174-182.

Jia, X., Ji, X., 2015. RSC Adv. 5, 107270-107275.

Jia, Y., Juarez, J., Li, J., Manuia, M., Niederst, M.J., Tompkins, C., Timple, N., Vaillancourt, M.-T., Pferdekamper, A.C., Lockerman, E.L., 2016. Cancer Res. 76, 1591-1602.

Lee, J.-H., Huh, Y.-M., Jun, Y.-w., Seo, J.-w., Jang, J.-t., Song, H.-T., Kim, S., Cho, E.-J., Yoon, H.-G., Suh, J.-S., 2007. Nat. Med. 13, 95-99.

Li, J., Qu, X., Payne, G.F., Zhang, C., Zhang, Y., Li, J., Ren, J., Hong, H., Liu, C., 2015. Adv. Funct. Mater. 25, 1404-1417.

Liu, D., Wang, L., Ma, S., Jiang, Z., Yang, B., Han, X., Liu, S., 2015. Nanoscale 7, 3627-3633.

Liu, G., Mao, X., Phillips, J.A., Xu, H., Tan, W., Zeng, L., 2009. Anal. Chem. 81, 10013-10018.

Pan, C., Guo, M., Nie, Z., Xiao, X., Yao, S., 2009. Electroanalysis 21, 1321-1326.

Pan, L.-H., Kuo, S.-H., Lin, T.-Y., Lin, C.-W., Fang, P.-Y., Yang, H.-W., 2017. Biosens. Bioelectron. 89, 598-605.

Parshetti, G.K., Lin, F.H., Doong, R.A., 2013. Sens. Actuators, B 186, 34-43.

Patra, S., Roy, E., Karfa, P., Kumar, S., Madhuri, R., Sharma, P.K., 2015. ACS Appl. Mater. Inter. 7, 9235-9246.

Qiu, J., Zhang, R., Li, J., Sang, Y., Tang, W., Gil, P.R., Liu, H., 2015. Int J Nanomedicine 10, 6709.

Qureshi, A., Gurbuz, Y., Niazi, J.H., 2012. Sens. Actuators, B 171, 62-76.

Seven, B., Bourourou, M., Elouarzaki, K., Constant, J.F., Gondran, C., Holzinger, M., Cosnier, S., Timur, S., 2013. Electrochem. Commun. 37, 36-39.

Shao, Y., Wang, J., Wu, H., Liu, J., Aksay, I.A., Lin, Y., 2010. Electroanalysis 22, 1027-1036.

Sun, Z., Fu, X., Zhang, L., Yang, X., Liu, F., HU, G., 2004. Anticancer Res. 24, 1159-1166.

Tabrizi, M.A., Shamsipur, M., Saber, R., Sarkar, S., 2017. Anal. Chim. Acta 985, 61-68.

Tangka, F.K., Howard, D.H., Royalty, J., Dalzell, L.P., Miller, J., O'Hara, B.J., Sabatino, S.A., Joseph, K., Kenney, K., Guy Jr, G.P., , 1997–2012 2015. Cancer Causes Control 26, 671.

Tsai, H.C., Doong, R.A., 2005. Biosens. Bioelectron. 20, 1796-1804.

Valeur, E., Bradley, M., 2009. Chem. Soc. Rev. 38, 606-631.

Wang, K., He, M.-Q., Zhai, F.-H., He, R.-H., Yu, Y.-L., 2017. Talanta 166, 87-92.

Wang, L., Ma, S., Wang, X., Liu, D., Liu, S., Han, X., 2013. J. Mater. Chem. B 1, 5021-5027.

Wang, Q., Jiao, L., Du, H., Wang, Y., Yuan, H., 2014a. J. Power Sources 245, 101-106.

Wang, X., Sun, X., Lao, J., He, H., Cheng, T., Wang, M., Wang, S., Huang, F., 2014b. Colloids Surf B Biointerfaces 122, 638-644.

Wu, S., He, Q., Zhou, C., Qi, X., Huang, X., Yin, Z., Yang, Y., Zhang, H., 2012. Nanoscale 4, 2478-2483.

Xie, J., Xu, C., Kohler, N., Hou, Y., Sun, S., 2007. Adv. Mater. 19, 3163-3166.

Zhang, Y., Luo, S., Situ, B., Chai, Z., Li, B., Liu, J., Zheng, L., 2018. Biosens. Bioelectron. 102, 568-573.

Zhao, J., Qiu, W., Simeone, D.M., Lubman, D.M., 2007. J. Proteome Res. 6, 1126-1138.

Zhou, L., Ge, X., Zhou, J., Wei, S., Shen, J., 2015. Chem. Commun. 51, 421-424.

Table 1. Analytical performance of ConA-GQD@Fe_3O_4 biosensing elements and other various electrochemical sensors for cancer cell detection:

Detection type	Method	Material	Linear range (cells mL^{-1})	Detection limit (cells mL^{-1})	References
Antibody or aptamer based sensor	EIS	Au/HS	10^4-10^7	6×10^3	Pan et al., 2009
		Graphene	10^3-10^6	794	Feng et al., 2011
		polypyrrole-GCEs[1]	100-10^5	100	Seven et al., 2013
		Au/Si	10^3-10^5	300	Chen et al., 2016
	DPV	MWCNTs-Pd_{nano}/PTCA[2]	10 - 5×10^5	21	Tabrizi et al., 2017
		polydA/AuNPs/GO	10-10^5	8	Wang et al., 2017
		dual catalytic hairpin assembly	50-10^5	30	Zhang et al., 2018
	ECL	RuSi@Ru(bpy)$^{3/2+}$ NP	56-5.6×10^6	56	Feng et al., 2014
		CdS-coated-ZnO	3×10^2-10^5	256	Liu et al., 2015
		TiO_2/CdS	4×10^2-10^4	396	Wang et al., 2013
		TU-capped MoS_2[3]	50–10^6	50	Guo et al., 2017
Biomolecular based sensor	EIS	Au/ConA	10^3-10^6	234	Hu et al., 2013
		ConA-GQD@Fe_3O_4	**5×10^2 - 10^5**	**246**	**This work**

GCE = glassy carbon electrode; MWCNTs-Pdnano/PTCA/aptamer = Multiwalled carbon nanotube/nano palladium/3,4,9,10-perylene tetracarboxylic acid; 3TU-capped MoS_2 = thiourea/Molybdenum sulfide.

Scheme 1. Schematic illustration of the preparation of ConA-GQD@Fe_3O_4 nanocomposites and the biosensing mechanism for cancer cell detection using ConA as the biosensing element to probe the glycoprotein and glycol on the cancer cell surface.

Fig. 1. (A) TEM image and (B) particle size distribution of as-synthesized GQDs, (C) HRTEM image of single GQD particle with lattice distance of 0.21 nm, TEM images of (D) Fe_3O_4 nanoparticles and (E) ConA-GQD@Fe_3O_4 nanocomposites, (F) HRTEM images of the ConA-GQD@Fe_3O_4 nanocomposites, (G) X-ray photoelectron spectroscopic (XPS) survey scan of Fe_3O_4 and GQD@Fe_3O_4 materials, (H) deconvoluted XPS N 1s peak of GQD@Fe_3O_4 nanocomposites, (I) TGA of the as-prepared Fe_3O_4 and GQD@Fe_3O_4, and (J) hydrodynamic diameters of GQDs, Fe_3O_4 and ConA-GQD@Fe_3O_4 nanocomposites.

Fig. 2. Cyclic voltammograms of Au||ConA-GQD@Fe_3O_4 electrode based on (A) different loading amounts of ConA ranging from 50 nM to 1 mM and (B) glucose interaction in the potential window of -0.2 – 0.6 V at a scan rate of 10 mV s^{-1} in 10 mM PBS solution at pH 7.4 containing 100 mM NaCl and 5 mM $Fe(CN)_6^{3-/4-}$; Nyquist plots of impedance spectra of Au||ConA-GQD@Fe_3O_4 electrodes before and after the incubation with different concentrations of (C) HeLa, (D) MCF-7, (E) MCF-10 and (F) bEnd.3 cells ranging from 500 to 100,000 cells mL^{-1} in the frequency range of 10,000 – 0.1 Hz with amplitude of 5 mV.

Fig. 3. Change in total impedance as a function of frequency before and after the addition of (A) HeLa, (B) MCF-7, (C) MCF-10 and (D) bEnd.3 cells in the concentration range of 0 – 10^5 cells mL^{-1} in the presence of Au||ConA-GQD@Fe_3O_4 electrode, (E) the percentage change in impedance and the linear relationship as a function of cell concentration in PBS

buffer; (F) fluorescence microscopic images of (i) HeLa and (ii) bEnd.3 cells with 20 μg mL^{-1} ConA-GQD@Fe_3O_4 nanocomposites at 37 °C for 4 h.

Fig. 4. Electrochemical performance and detection of circulating tumor cells (CTCs) collected from blood samples. (A) Nyquist plot, (B) total impedance, and (C) concentration of calculated cells based on the calibration line found in PBS buffer.

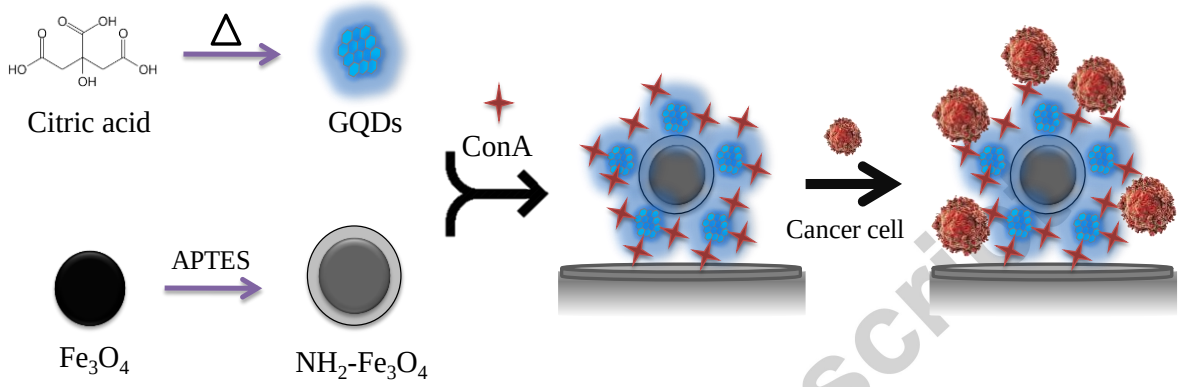

Scheme 1.

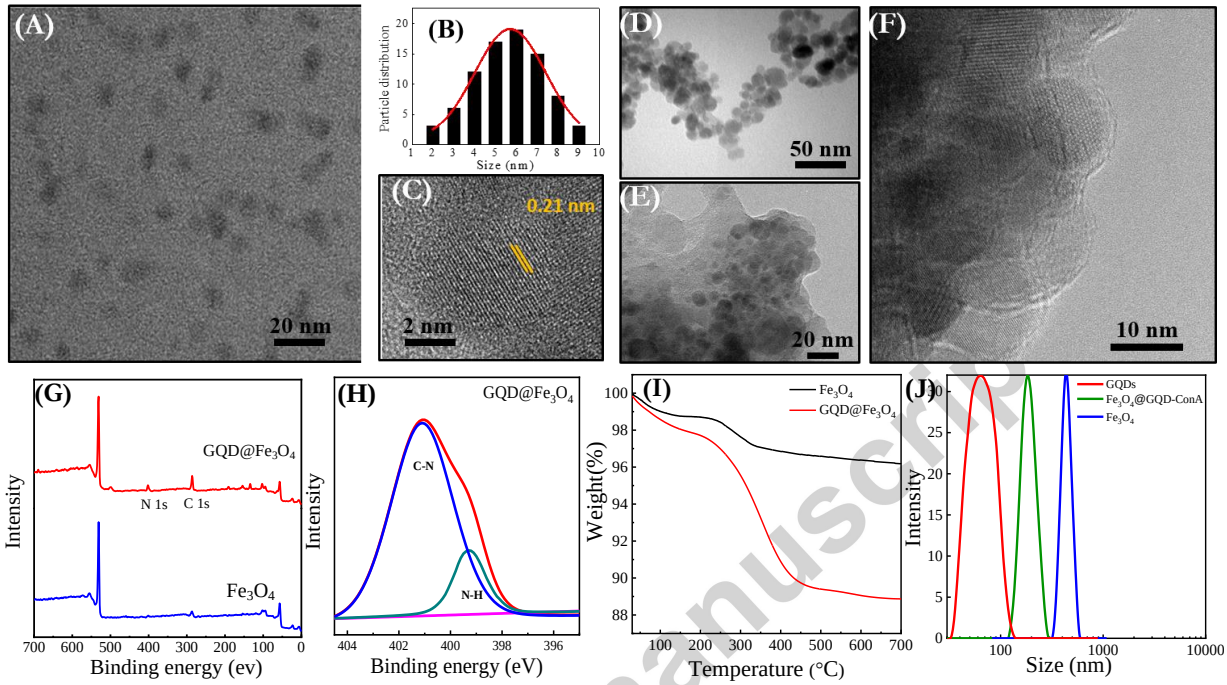

Fig. 1

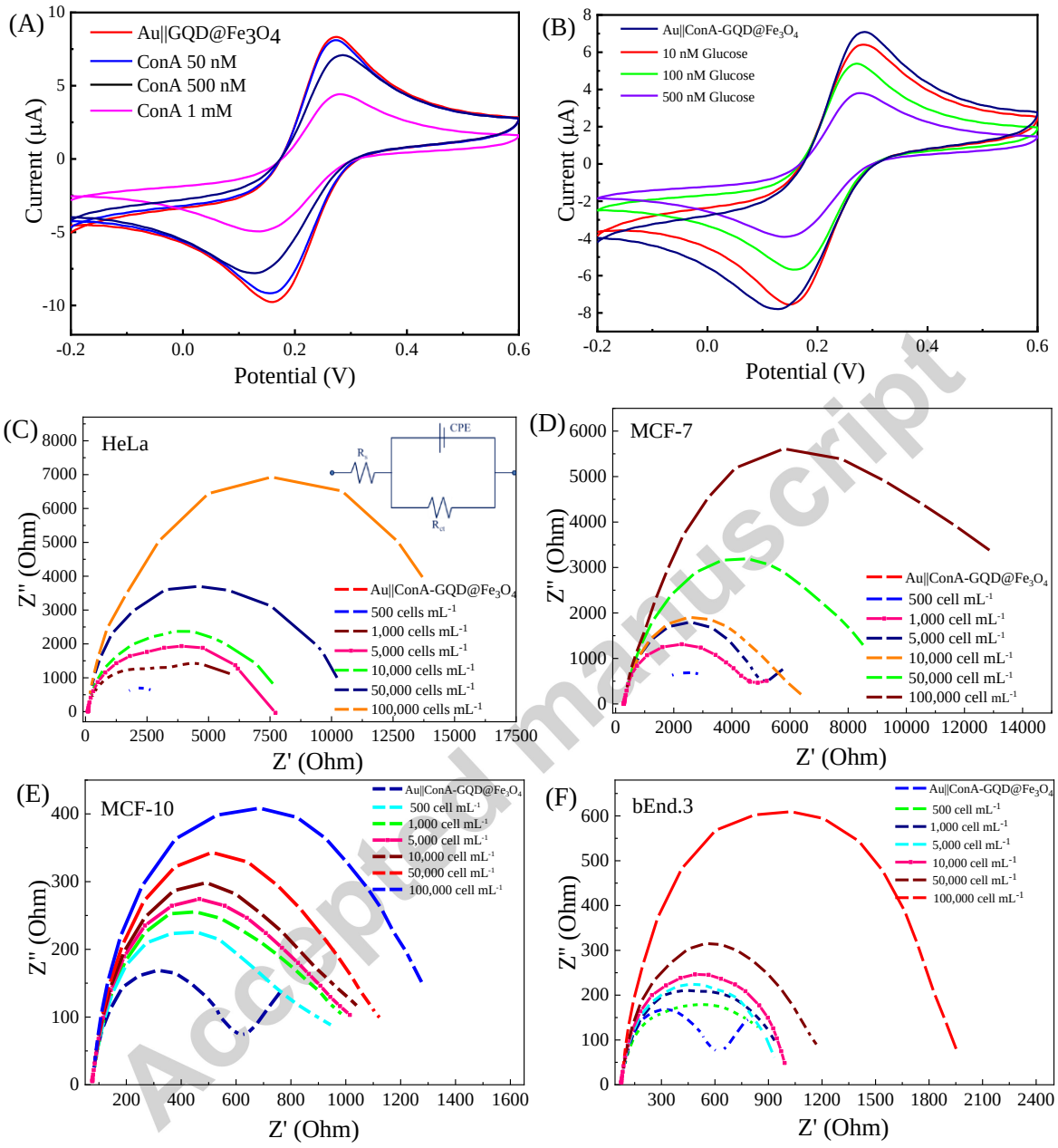

Fig. 2.

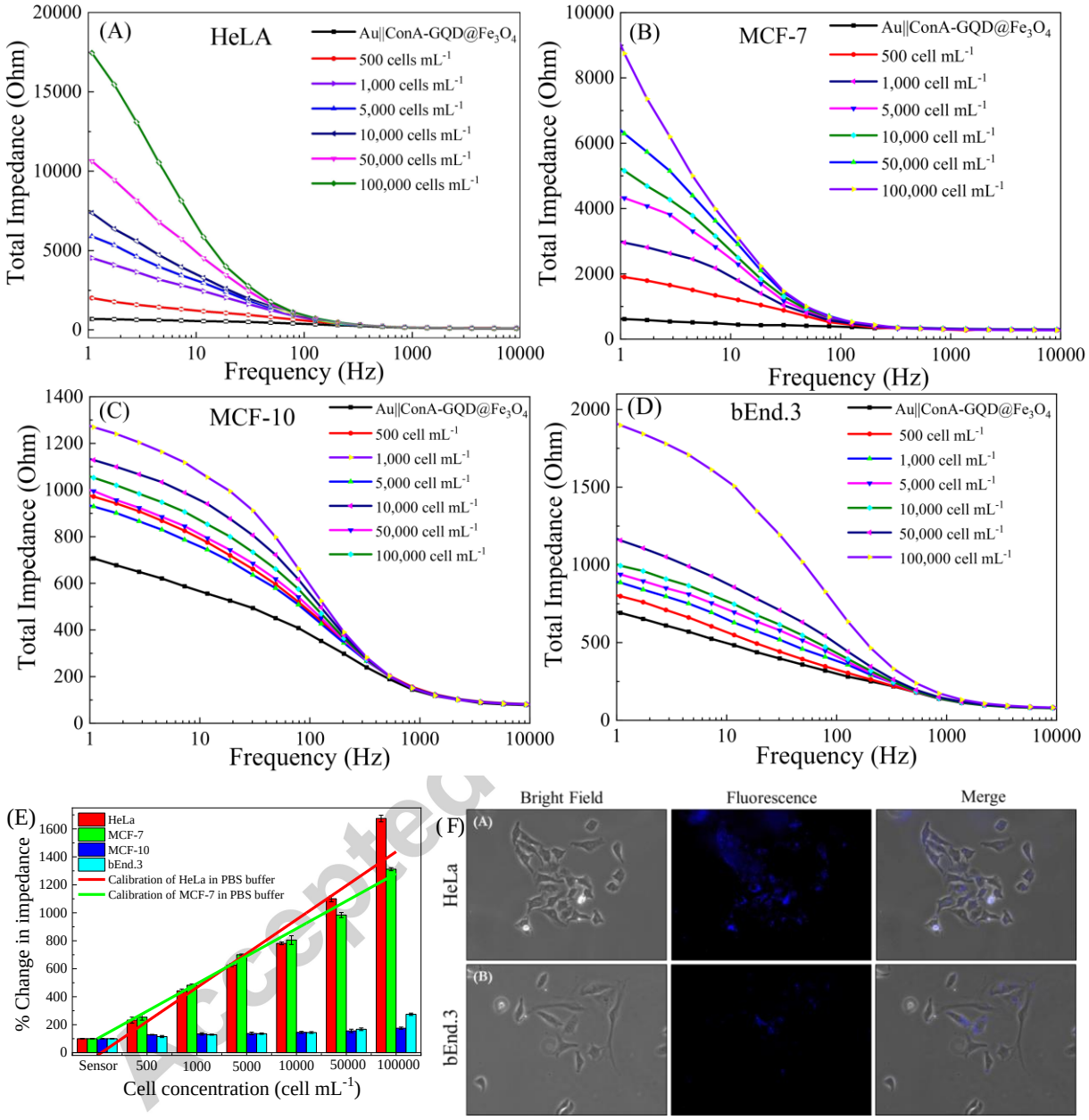

Fig. 3.

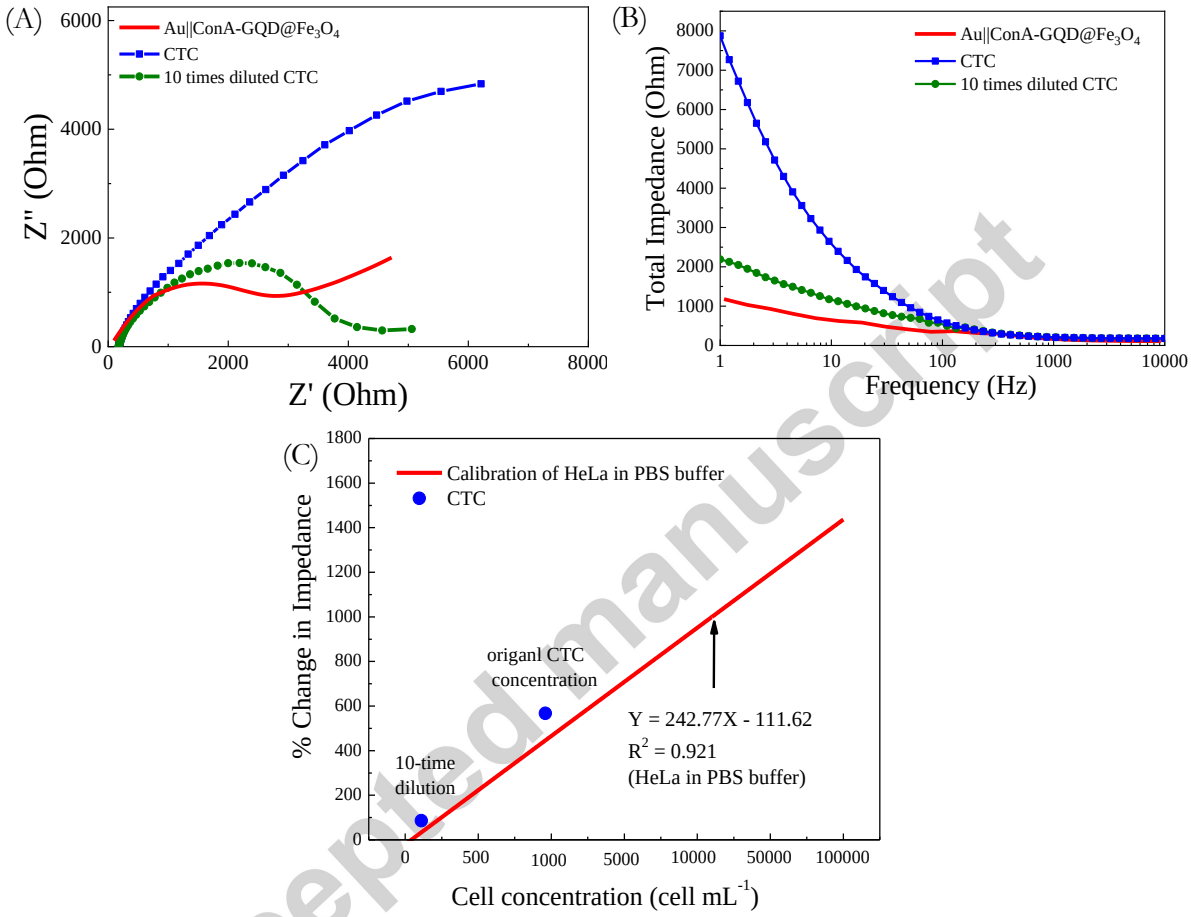

Fig. 4.

Highlights

- Label-free ConA-GQD@Fe_3O_4 biosensor for impedimetric cancer cell detection
- Using specific binding of ConA toward overexpressed glycogenated cancer cell surface, selectivity achieved
- Distinct impedimetric response for cancerous HeLa, MCF-7 whereas nonconcarous MCF-10, bEnd3 are ignorable
- A linearity found in $5 \times 10^2 - 1 \times 10^5$ cells mL^{-1} with LOD of 246 and 367 cells mL^{-1} for HeLa and MCF-7